IEEE Access
Multidisciplinary | Rapid Review | Open Access Journal

Received March 21, 2020, accepted April 2, 2020, date of publication April 7, 2020, date of current version April 22, 2020.

Digital Object Identifier 10.1109/ACCESS.2020.2986265

An Adaptive Cross-Validation Thresholding De-Noising Algorithm for Fault Diagnosis of Rolling Element Bearings Under Variable and Transients Conditions

YI LIU[1,2], ZHANSI JIANG[2], AND JIAWEI XIANG[1], (Member, IEEE)
[1]College of Mechanical and Electrical Engineering, Wenzhou University, Wenzhou 325035, China
[2]School of Mechanical and Electrical Engineering, Guilin University of Electronic Technology, Guilin 541004, China

Corresponding author: Jiawei Xiang (jwxiang@wzu.edu.cn)

This work was supported in part by the National Natural Science Foundation of China under Grant U1909217, U1709208, in part by the Zhejiang Special Support Program for High-Level Personnel Recruitment of China under Grant 2018R52034, and in part by the Wenzhou Key Innovation Project for Science and Technology of China under Grant 2018ZG023 and Grant ZG2019018.

ABSTRACT Developing a proper approach for extracting the fault characteristics of rolling element bearings is a significant behavior in variable operation conditions. Generally, without a tachometer, the tacholess order tracking method is well established by instantaneous rotation frequency curve estimation using time-frequency analysis. However, the fault features are often masked in strong background noises. An adaptive cross-validation thresholding de-noising algorithm is employed to improve the performance of the traditional envelope order spectrum method. First, the general linear chirplet transform is applied to estimate the instantaneous rotation frequency curve. Second, with the help of the instantaneous rotation frequency curve, the raw non-stationary signal is transferred to an angular domain by the re-sampling technique. Third, the adaptive cross-validation thresholding de-noising algorithm is employed to purify the angular domain signal to improve the fault feature extraction performance of the envelope order spectrum method. Comparisons using numerical simulations and experimental investigations of bearing faults under variable speed conditions are given to show the superiority of the present method.

INDEX TERMS Amplitude modulation, frequency modulation, band-pass filter, frequency estimation, spectral analysis, signal de-noising, signal restoration, fault diagnosis.

I. INTRODUCTION

Rolling element bearings are one of the core elements of rotating motion in mechanical systems, such as planetary gearbox transmissions and motor devices [1]–[7]. Bearings are prone to failure in mechanical systems.

In recent years, a state-of-the-art investigation indicates that more extracted fault information is exposed under time-varying condition than under a constant speed condition [8]. Variable operation conditions of mechanical systems, for example, speeding up or slowing down and variable load conditions are often found in industrial applications [9]. Therefore, vibration signal properties are non-stationary and nonlinear, which increase the difficulty of fault detection.

The associate editor coordinating the review of this manuscript and approving it for publication was Gerard-Andre Capolino.

Computed order tracking (COT) [10] is applied to transfer the non-stationary domain into the quasi-stationary domain to eliminate the influence of speed variation. However, due to the installation limitations and high costs, this technique is replaced by tacholess order tracking (TLOT), which does not require any hardware equipments. TLOT method depends on the obtained instantaneous rotation frequency (IRF) curve for rolling element bearing fault diagnosis under variable speed conditions [11]–[14].

Time-frequency analysis (TFA) methods have the ability to characterize the variation procedure of a signal. Conventional TFA methods included the short time Fourier transform (STFT), wavelet transform (WT) and Wigner-Ville distribution (WVD) in the past decades [15]–[20]. The STFT and WT suffer from Heisenberg uncertainty principle [21]. The WVD always introduces cross-term interferences while analyzing

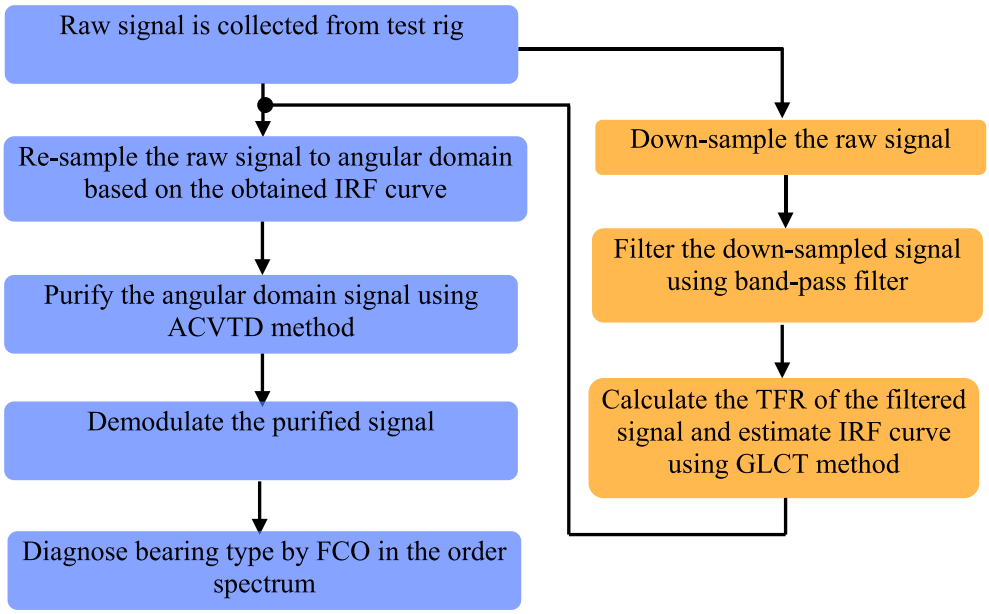

FIGURE 1. Flowchart of ACVTD based EOS method for bearing fault detection under variable speed conditions.

the multi-component signal. To overcome this drawback, Yu and Zhou [22] proposed the generalized linear chirplet transform (GLCT) method, which well characterizes the multi-component signal in non-stationary conditions and no longer preset the chirp rate of non-linear signal; meanwhile, it can provide high IRF resolution and retreat the drawbacks of conventional TF analysis methods.

By means of the obtained IRF curve, the envelope order spectrum (EOS) method is employed to extract the fault characteristic order (FCO) of vibration signals. Unfortunately, the fault features are polluted by unrelated components and cannot be directly recognized. Recently, many researchers have applied some methodologies to separate fault features from the angular domain signal. Wang *et al.* [23] developed a hybrid method, which applied COT and variational mode decomposition (VMD) –based time frequency representation (VTFR) for fault detection. However, the input parameters (balancing parameter and the number of modes) are the key factors of VMD, which need be predetermined. Reference [24] applied the maximum correlated kurtosis de-convolution (MCKD) method to enhance the fault features of the angular domain signal and then by means of the EOS method obtain the FCO of the tested rolling element bearings. Similarly, the fault period should be preset as a crucial parameter in signal de-noising processing. Wang and Xiang [25] introduced the angle synchronous averaging (ASA) technique into the angular domain signal and then the fault features are recognized using EOS method. This method simultaneously weakens the energy of unrelated and fault components. The weak fault diagnosis method for rolling bearing under variable speed conditions using the improved empirical wavelet transform (IEWT)-based enhanced envelope order spectrum is proposed in [26], in which cuckoo search algorithm (CSM) was also used to determine the support interval of the EWT to ensure the accuracy of the angular domain signal decomposition. Although this avoided presetting related parameters, it increased the computation complexity.

Adaptive cross-validation thresholding de-noising (ACVTD) is applied to eliminate the additive noise of the seismic signal for preserving important features [27], [28], i.e., extracting P- and S-waves from seismic signals. The localized defect of the surface of rolling bearings occurs in operation, and if the rolling element moves over the damaged area, the vibration signal would appear as a transient impulse, which is similar to P- and S-waves from seismic signals. This hybrid method is first applied in fault diagnosis areas.

The method ACVTD consists of two main steps, they are kurtosis criterion and synchrosqueezed-continuous wavelet transform (SS-CWT). Kurtosis criterion is a preprocessing to select the transient impulse components of the vibration signal. Furthermore, the processed signal is transformed in the SS-CWT domain, in which the major oscillatory components is distinguished and the high-power coherent noise outside of the frequency range is removed. In summary, the method has the ability of fault components extraction. To meet the actual industrial application, the algorithm is applied under variable speed conditions. The speed information acquisition using TFA method without installing tachometer, which could decrease cost and avoid the difficult of installation of the equipment.

The remainder of this paper is arranged as follows: the theories of ACVTD and GLCT are briefly reviewed in section II. The proposed method is given in section III. The effectiveness of the proposed method is validated by some simulations and experiments in section IV and section V, respectively. The discussion is shown in section VI. Finally, conclusion is given in section VII.

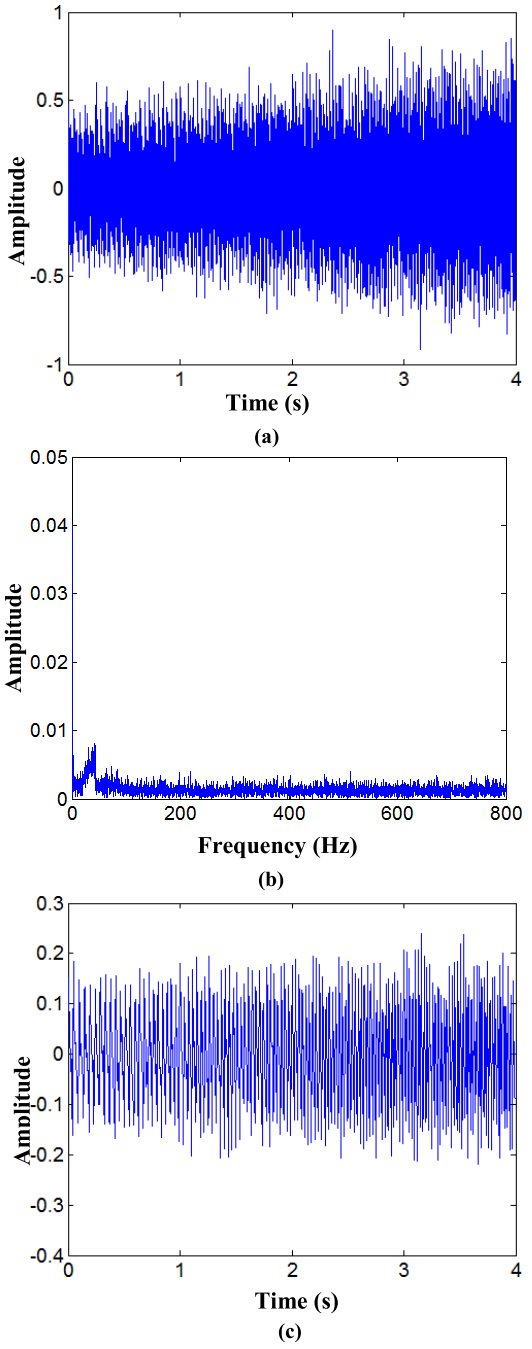

FIGURE 2. Simulated faulty raw signal (with SNR of −3.6 dB) under variable speed conditions: (a) waveform of the raw signal, (b) spectrum of the raw signal, (c) waveform of the down-sampled signal.

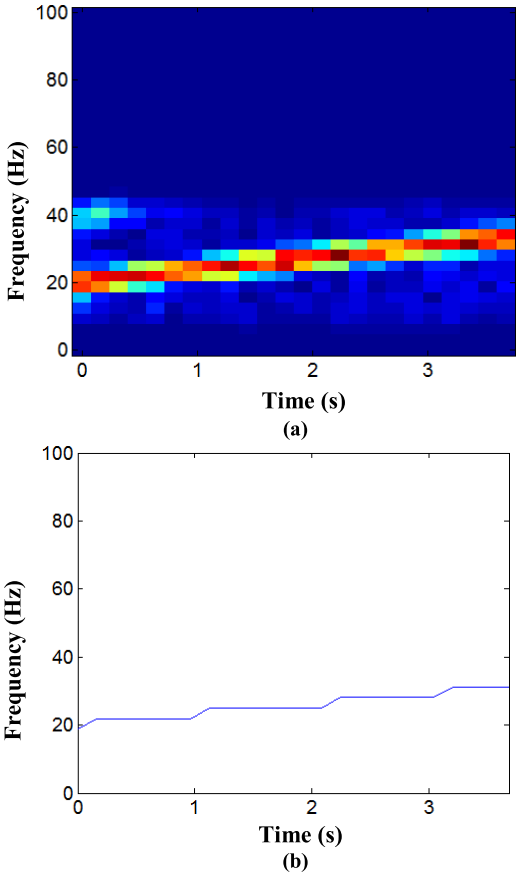

FIGURE 3. Simulated faulty raw signal (with SNR of −3.6 dB): (a) spectrogram of the raw signal based STFT, (b) estimation IRF curve based the obtained TFR by STFT.

II. THEORETICAL BACKGROUND

A. THE PRINCIPLE OF THE ADAPTIVE CROSS VALIDATION THRESHOLDING DE-NOISING ALGORITHM

This algorithm consists of two stages: preprocessing and cross-validation thresholding. In this part, the stages of the algorithm are described. CWT is a multi-resolution time-frequency transform method, which is widely used in industrial fields [29], [30]. It can avoid the selection of the window length to ensure a tradeoff between time and the frequency resolution. The CWT of signal $y(t)$in Eq. (1) at scale a and time shift b is given by:

$$X_y(a,b) = \langle y, \phi_{a,b} \rangle = \frac{1}{\sqrt{a}} \int_{-\infty}^{+\infty} y(t)\phi^*(\frac{t-b}{a})\mathrm{d}t \quad (1)$$

where $X_y(a,b)$ is a wavelet coefficient, $\langle y, \phi_{a,b} \rangle$ is the inner product, and * denotes the complex conjugate. In the frequency domain, Eq. (1) can be written as

$$X_y(a,b) = \frac{1}{2\pi} \int_{-\infty}^{+\infty} \tilde{y}(\psi) a^{-\frac{1}{2}} \tilde{\phi}^*(a\psi) e^{(j\psi b)} \mathrm{d}\psi \quad (2)$$

where $\tilde{y}(\psi)$ is the Fourier transform of $y(t)$. The inverse CWT is given by [31]

$$y(t) = \frac{1}{C_\phi} \iint X_y(a,b)\mathrm{d}b\frac{\mathrm{d}a}{a^2} \quad (3)$$

where $C_\phi = \int_0^{+\infty} \psi^{-1}\tilde{\phi}^*(\psi)\mathrm{d}\psi$.

However, the variable length of ϕ results in a flexible tradeoff between time and the frequency resolution compared with the STFT. The SS technique is introduced by squeezing the energy around ridges to decrease smearing, which has a superior frequency resolution, and then could distinguish the major oscillatory components of vibration signals [32]–[34]. The synchrosqueezed transform (SST) is

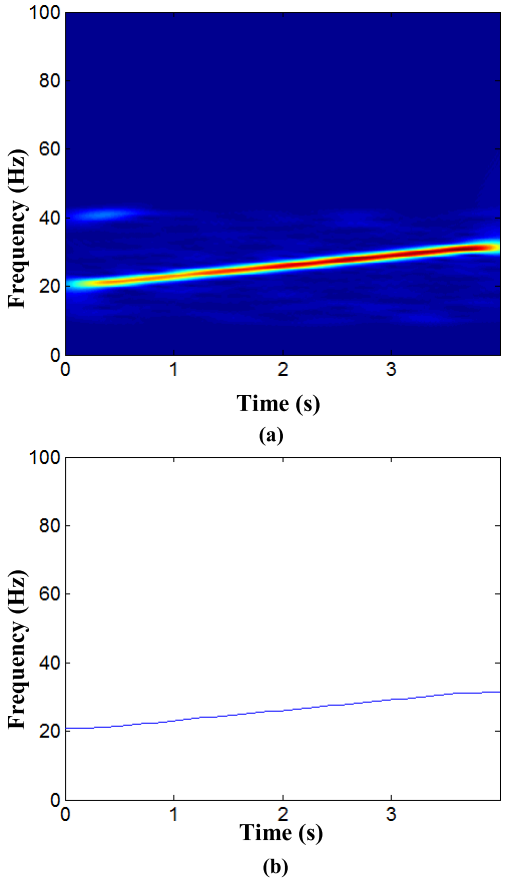

FIGURE 4. Simulated faulty raw signal (with SNR of −3.6 dB): (c) spectrogram of the raw signal based GLCT, (d) the estimation IRF curve based on the obtained TFR by GLCT.

represented as Eq. (4):

$$T_y(\omega_l, b) = (\Delta\omega)^{-1} \sum_{a_k|\omega(a_k,b)-\omega_l|\le\Delta\omega/2} X_y(a_k, b) a_k^{-3/2} \Delta a_k \quad (4)$$

The parameters of this formula are shown. First we need to obtain the coefficients $X_y(a, b)$ at discrete value a_k, which is the k^{th} scale, and $a_k - a_{k-1} = \Delta a$. Similarly, ω_l is defined as the discrete frequencies, with $\omega_l - \omega_{l-1} = \Delta\omega$. $l \in L_k(t)$ denotes the k^{th} component in a small band frequency. The inverse of $T_y(\omega_l, b)$ is obtained as:

$$y_k(t) = 2C_\phi^{-1} \,\text{Re}\Big(\sum_{l\in L_k(t)} T_y(\omega_l, b)\Big) \quad (5)$$

In the first step of preprocessing, the vibration signal $y(t)$ is transformed into the SS-CWT domain, and the high power coherent noise is removed from the TFR of the signal using the kurtosis criteria Eq. (6) and Eq. (7) (for distinguishing a Gaussian distribution from a non-Gaussian distribution). The formulas are shown below:

$$kurt = \frac{\sum_{n=1}^{N} (X_{yn} - E(X_y))^4}{N\sigma_{X_y}^4} - 3 \quad (6)$$

$$|kurt| \le \frac{\sqrt{24/N}}{\sqrt{1-\alpha}} \quad (7)$$

where σ is the denoted the standard deviation, E represents the mean of X_y, and α is the level of confidence, which is commonly set to 0.9.

The simplest but most popular threshold rule is soft-threshold, which is given by

$$\varepsilon_\lambda^s(X_y) = \text{sgn}(X_y).(|X_y| - \lambda)_+ \quad (8)$$

where sgn(.) is the sign function, and the threshold λ is found by the cross-validation (CV) method. A data point is systematically excluded from the construction of an estimate, and then the value of the excluded data point is predicted and compared with the true value. The function of CV is defined as

$$CV(\lambda) = \frac{1}{N} \frac{\left\| T_y - \widehat{T}_\lambda \right\|^2}{\left\| \frac{N_0}{N} \right\|^2} \quad (9)$$

where $\widehat{T}_\lambda$ are the threshold coefficients using a threshold value of λ, and N_0 is the number of coefficients that would be zeroed using the threshold value λ. In the second step, the obtained preprocessed coefficients are thresholded by the soft-threshold method. In the SS domain, Eq. (8) is used to threshold the major oscillatory components of the signal in a narrow frequency band and the optimal threshold λ_0 (the Fibonacci method is used to find this value) is automatically determined by the CV method for each narrow frequency. On the basis of finishing the thresholding of the major oscillatory components, we obtain an initial estimate of the signal using the inverse transform from Eq. (5). As a consequence, the raw signal is de-noised by ACVTD.

B. THE PRINCIPLE OF THE GENERALIZED LINEAR CHIRPLET TRANSFORM

It is well-known the formula of linear chirplet transform (LCT) [35], which can be expressed by Eq. (10). In this paper, the tested signals are non-stationary, LCT method could effectively provide chirp rate to characterize the speed variation signal. We assume a vibration signal is $y(t)$ and LCT is obtained as

$$S(t', \omega, c) = \int_{-\infty}^{+\infty} g(\tau - t) y(\tau) e^{-j\omega\tau} e^{\frac{-jc(\tau-t)^2}{2}} d\tau \quad (10)$$

where the parameters c and g represent the chirp rate and the window function respectively. The demodulated operator $e^{-jc(\tau-t)^2/2}$ will produce a rotating effect in the time-frequency plane, and its rotating degree is $\arctan(-c)$. We assume the sampling frequency is F_s and the sampling time is T_s. The parameter c is determined as

$$c = \frac{F_s \tan(\alpha)}{2T_S}, \quad \alpha \in (-\pi/,2, -\pi/2,) \quad (11)$$

and Eq. (11) can be rewritten as

$$S(t, \omega, \alpha) \int_{-\infty}^{+\infty} g(\tau - t) y(\tau) e^{-j\omega\tau} e^{-j.\frac{\tan(\alpha).(\tau-t)^2}{4T_s} F_s} d\tau \quad (12)$$

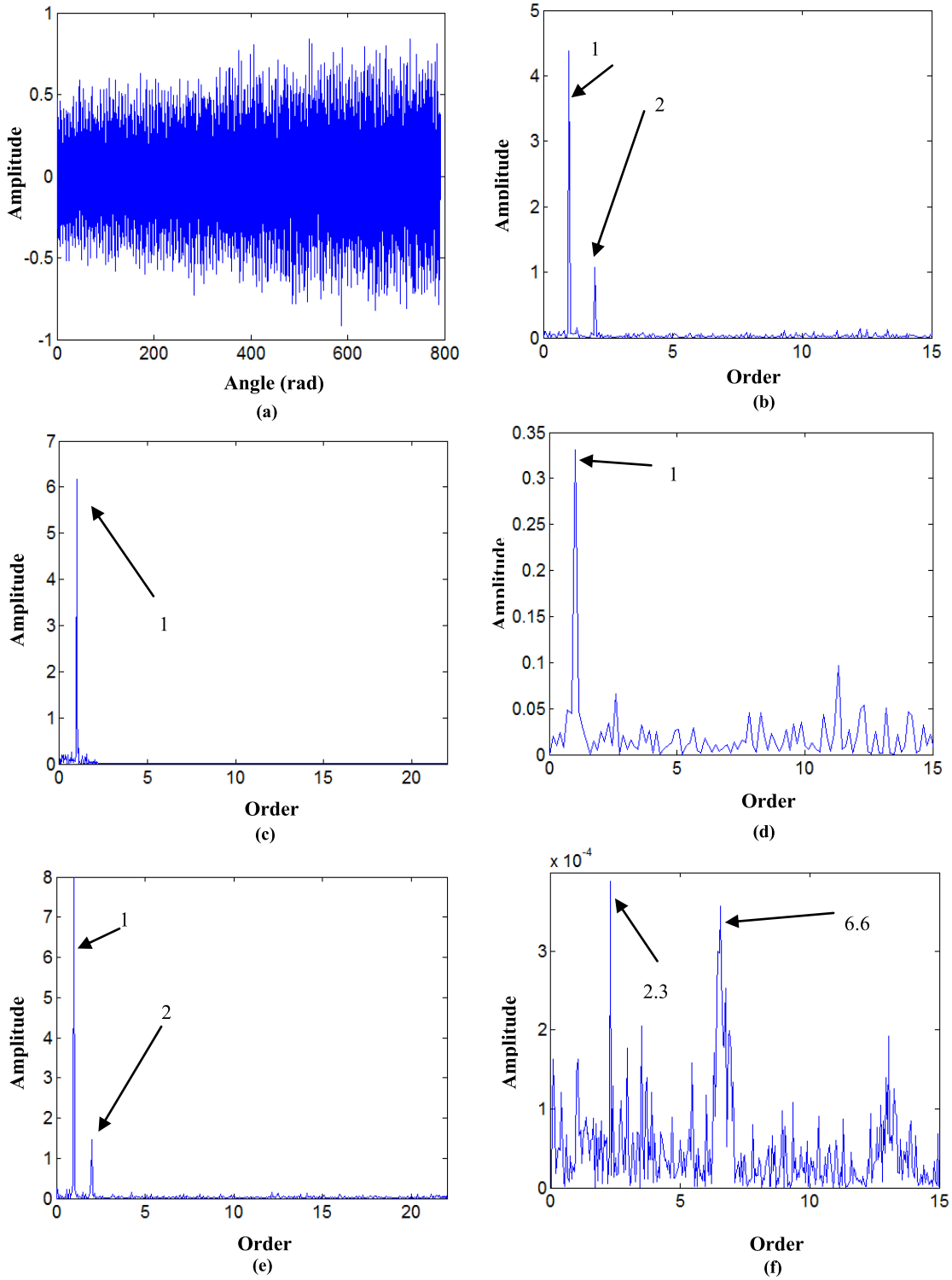

FIGURE 5. Angular domain signal (with SNR of −3.6 dB): (a) waveform of the angular domain signal, (b) order spectrum of the angular domain signal, (c) order spectrum of AW output signal, (d) order spectrum of ASA output signal, (e) order spectrum of WHT output signal, (f) order spectrum of ACVTD output signal.

Eq. (12) is for GLCT method, all feasible modulated elements in the signal can be described by demodulated operators. Subsequently, the parameter α is determined by the number of segments denoted by N. The equation can be

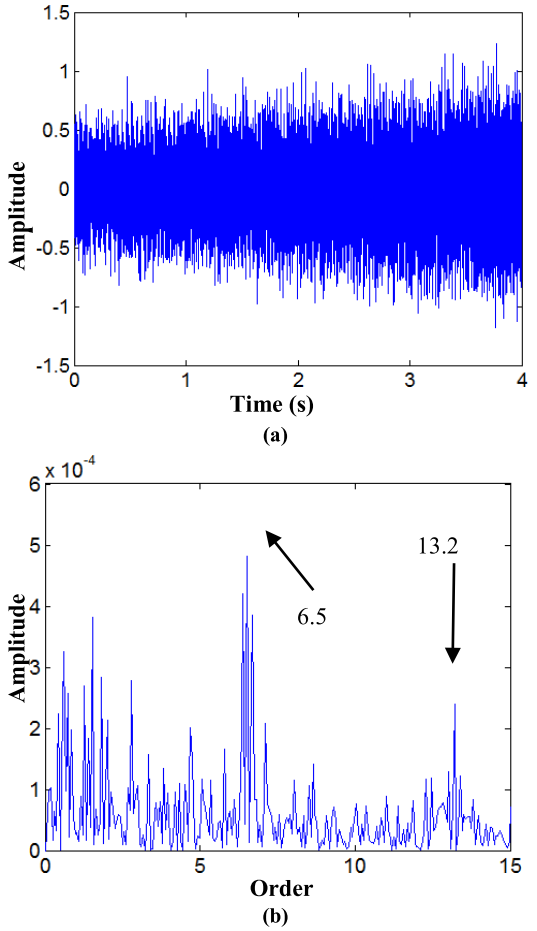

FIGURE 6. Simulated faulty raw signal (with SNR of −6.9 dB) under variable speed conditions: (a) waveform of the raw signal, (b) order spectrum of the ACVTD output signal.

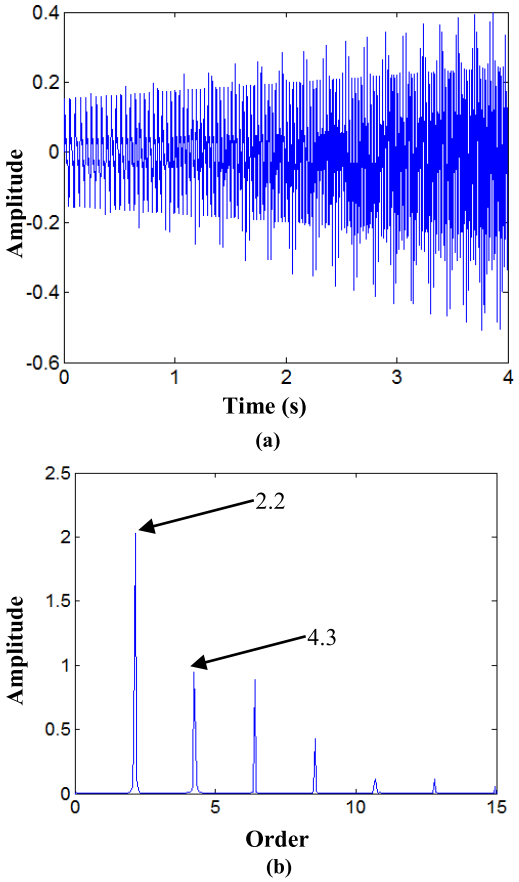

FIGURE 7. Simulated faulty raw signal (with SNR of 0 dB) under variable speed conditions: (a) waveform of the raw signal, (b) order spectrum of the ACVTD output signal.

shown as:

$$\alpha = \begin{cases} -\pi/2 + 1 \cdot \pi/(N+1), \\ -\pi/2 + 2 \cdot \pi/(N+1) \\ \cdots \\ -\pi/2 + N \cdot \pi/(N+1) \end{cases} \tag{13}$$

$$c' = \arg\max_{c} |S(t, \omega, c)| \tag{14}$$

If $N = 1$, Eq. (12) will degenerate to the STFT [16]. The value c' is denoted as the optimal value of c, which is determined by Eq. (14). The final result can be defined as

$$S(t, \omega) = S(t, \omega, c') \tag{15}$$

That method utilizes a series of discrete demodulated operators to characterize the instantaneous rotation frequency feature rather than construct a mathematical model.

III. THE ACVTD BASED EOS

The fault diagnosis method consists of two steps. The first step is to transform the time domain into the angular domain by the re-sampling technique based on the estimated IRF curve. The second step is to purify the angular domain signal by ACVTD, and then use EOS method to recognize the fault types. The flowchart of the proposed method under variable speed conditions is shown in Fig. 1.

A. DATA ACQUISITION

Collect data from the test rig under variable speed conditions.

B. DOWN-SAMPLE THE COLLECTED RAW SIGNAL

For IRF curve estimation of the shaft, we decimate the raw sampling frequency at lower values to eliminate redundant information. If the range of the IRF is less than 100 Hz in data acquisition processing we decimate the raw sampling frequency at 200 Hz.

C. FILTER THE PROCESSED SIGNAL

We introduce band-pass filter to remove IRF harmonics of the down-sampled signal. The related parameters are set, which based on the range of the rotation frequency in the data acquisition experiment for different cases.

D. CALCULATE THE TFR OF THE FILTERED SIGNAL AND THEN EXTRACT THE IRF CURVE

The GLCT method has the ability to characterize speed variations and provides a high quality time-frequency resolution of the IRF of shafts. When the optimal chirp rate is reached,

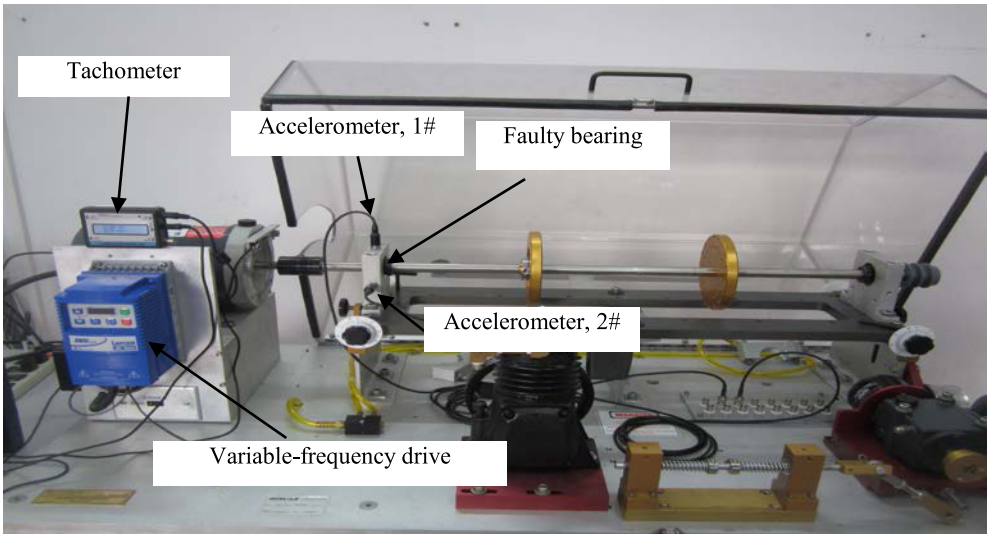

FIGURE 8. Machinery fault simulator test rig.

the maximum amplitude $|S(t, \omega, \alpha)|$ is obtained. With the help of the estimated IRF, the ridge extraction method is applied to extract it.

E. RE-SAMPLE THE RAW SIGNAL INTO THE ANGULAR DOMAIN

The new sampling frequency is variable while speed of shaft changes. Apply the re-sample technique to transform the non-stationary signal into a quasi-stationary signal with the even-angle increments.

F. PURIFY THE ANGULAR DOMAIN SIGNAL BY ACVTD

The angular domain signal still contains unrelated components, such as background noises. ACVTD is applied to remove them and highlight the fault components.

G. FAULT FEATURES ARE EXTRACTED

The fault characteristic orders are detected using the EOS method. The analytic and envelope of the angular domain signal $v_i(\theta)$ are given by

$$z_i(\theta) = v_i(\theta) + j\widehat{v}_i(\theta) \tag{16}$$

$$a_i(\theta) = \sqrt{v_i^2(\theta) + \widehat{v}_i^2(\theta)} \tag{17}$$

IV. NUMERICAL SIMULATION

In this section, a numerical simulation of the corresponding defective rolling element bearing under variable speed conditions is given and further to verify the effectiveness of the proposed method for fault diagnosis. The speed of the simulated signal is variable, and the formula can be given as Eq. (18) and Eq. (19):

$$y(t) = A_n \sum_{n=0}^{+\infty} e^{(-b(t-T_n-\tau_n))} \cos(2\pi f_n(t - T_n - \tau_n)) + \sigma(t) \tag{18}$$

where A_n denotes the amplitude of the n^{th} impulse, b is the structural damping characteristic, T_n represents the interval time between the $(n-1)^{\text{th}}$ and $(n+1)^{\text{th}}$ impulses, $\tau_n$denotes the random slippage of rolling elements, for which the range is from 0.01 to 0.02, f_n represents the natural frequency, and $\sigma(t)$ is an added white Gaussian noise with a signal-to-noise ratio (SNR) of -3.6 dB. To verify the de-noising effectiveness of the proposed method, we will add different white Gaussian noises with SNR values of -6.9 dB and 0 dB into the simulated signal and keep other parameters constant.

We assume the fault occurrence time with the speed variation is

$$\begin{cases} t_1 = (1 + \tau_1) \times 1/\left(f_r\left(t_0\right)\right)/B \\ t_n = (1 + \tau_n) \times n/\left(f_r\left(t_{n-1}\right)\right)/B, \quad n = 2, 3... \end{cases} \tag{19}$$

where $f_r(t)$ is the instantaneous rotation frequency, B represents the fault characteristic order and t_n is the occurrence time of the n^{th} impulse. In this formula, we consider the influence of slippage of the rolling elements.

The specific parameters of the numerical simulation are $t = [0, 4]s$, $A_n = \lambda \times t_n$ (λ is a constant value, which equals -0.091), $b = 1000rad/s$, $B = 2.2$, $\tau_n = 0.02$, $f_0 = 6500Hz$, and $f(t) = 3t + 20$. The sampling frequency is 12 kHz.

The simulated signal and its Hilbert envelope spectrum are shown in Fig. 2(a) and (b), respectively. From the Fig.2 (b), the smear spectrum is smeared due to the speed variation, and we cannot detect fault features. The waveform of the down-sampled signal is shown in Fig. 2(c).

For fault detection, the raw signal is down-sampled and the original sampling frequency is decimated at $f_s \times (1/60)$. According to the above mentioned $f_r = 3t + 20$ and $t \in [0, 4]$, we obtain the range of the rotation frequency $f_r \in [20, 32]$. Therefore, the central frequency and bandwidth frequency parameters of the band-pass filter are 32 Hz and 28 Hz, respectively. Fig. 3(a) and (b) show the obtained time-frequency representation (TFR) of the filtered signal

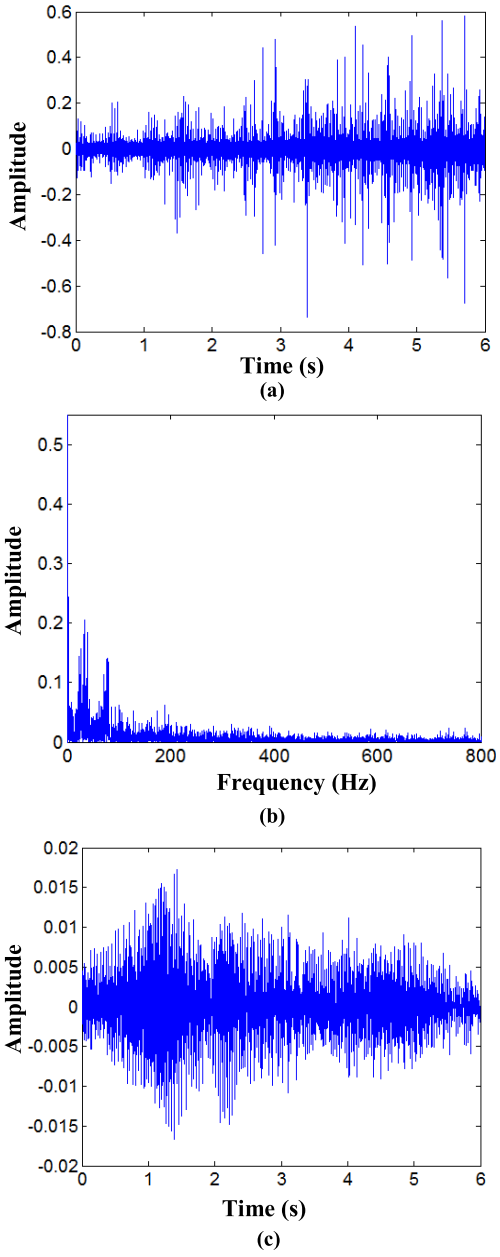

FIGURE 9. Raw signal of rolling element bearing with an inner race fault under variable speed conditions: (a) waveform of the raw signal, (b) spectrum of the raw signal, (c) waveform of the down-sampled signal.

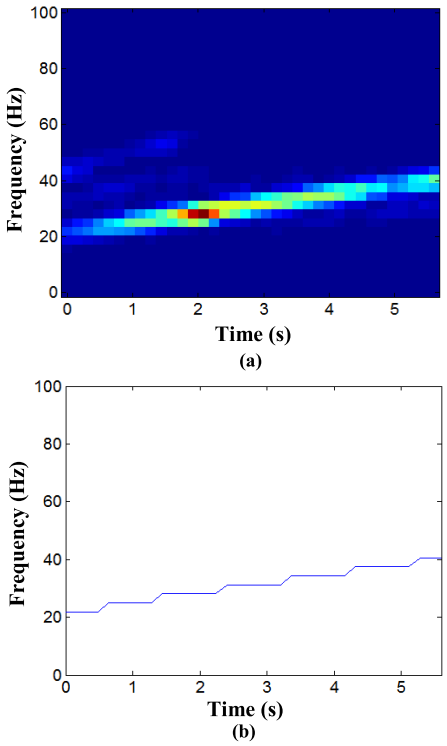

FIGURE 10. Rolling element bearing with an inner race fault: (a) spectrogram of the raw signal based STFT, (b) estimation IRF curve based the obtained TFR by STFT.

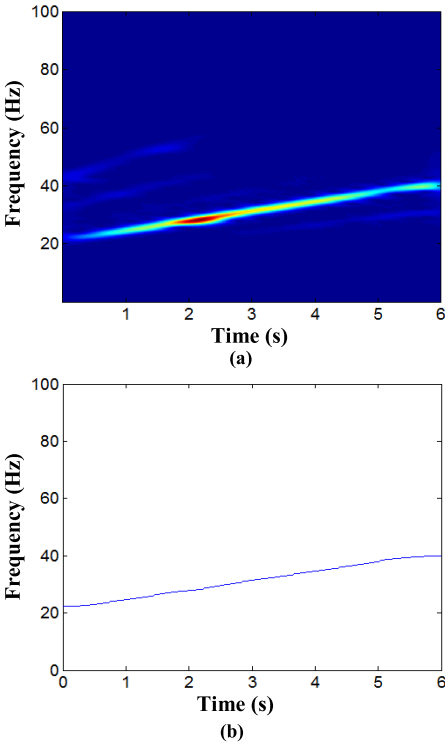

FIGURE 11. Rolling element bearing with an inner race fault: (a) spectrogram of the raw signal based GLCT, (b) estimation IRF curve based the obtained TFR by GLCT.

based on STFT and its corresponding IRF curve. Obviously, the inaccuracy of the IRF curve is estimated due to the low quality time-frequency resolution. The TFR of the filtered signal by GLCT is shown in Fig. 4 (a), and the estimated IRF curve is shown in Fig. 4(b), which validly characterizes the tendency of the rotation frequency. The re-sampling technique is applied to transform the raw signal into the angular domain signal based on the estimated IRF curve, and furthermore, the re-sample frequency is obtained by the formula $O_s = f_s/f_{r\,\min} = 569.34$.

The angular domain signal and its order spectrum are shown in Fig. 5(a) and (b), respectively, and only the shaft orders 1 and 2 are recognized. The automated wavelet (AW) algorithm is used to remove noise components in the vaginal pulse amplitude signal, which is equally applied to remove

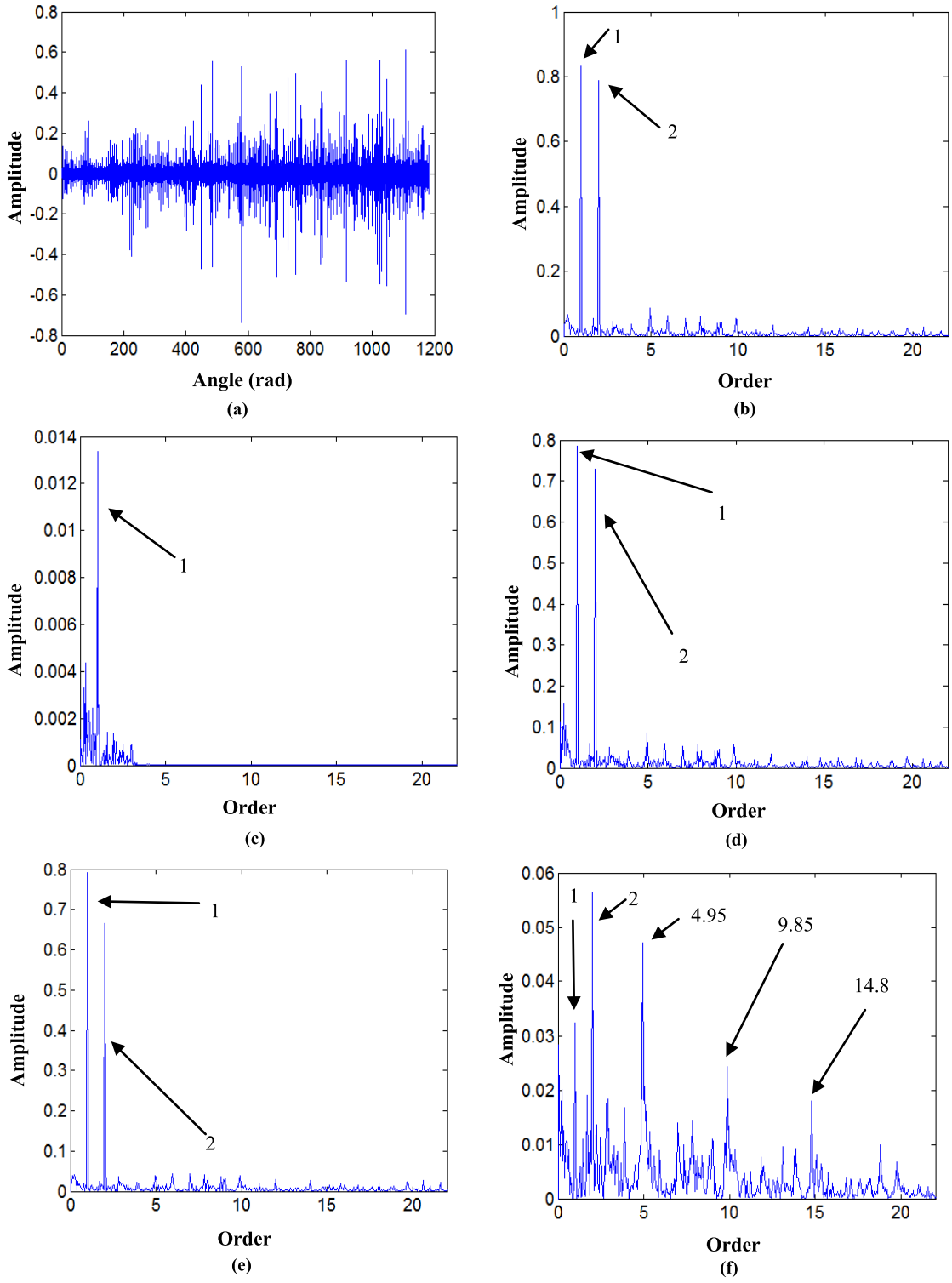

FIGURE 12. Angular domain signal: (a) waveform of the angular domain signal, (b) order spectrum of the angular domain signal, (c) order spectrum of AW output signal, (d) order spectrum of ASA output signal, (e) order spectrum of WHT output signal, (f) order spectrum of ACVTD output signal.

interference noise in the raw signal. Angle synchronous averaging (ASA) is applied as a preprocess step to weaken the energy of unrelated components, such as the background noises. A conventional de-noising method based on multi-resolution analysis called the wavelet hard-threshold (WHT) method is applied to filter the signal, and in this paper, the ''dB4'' wavelet function is used. From Fig. 5(c), only the shaft order 1 is detected, and the obtained result is the order

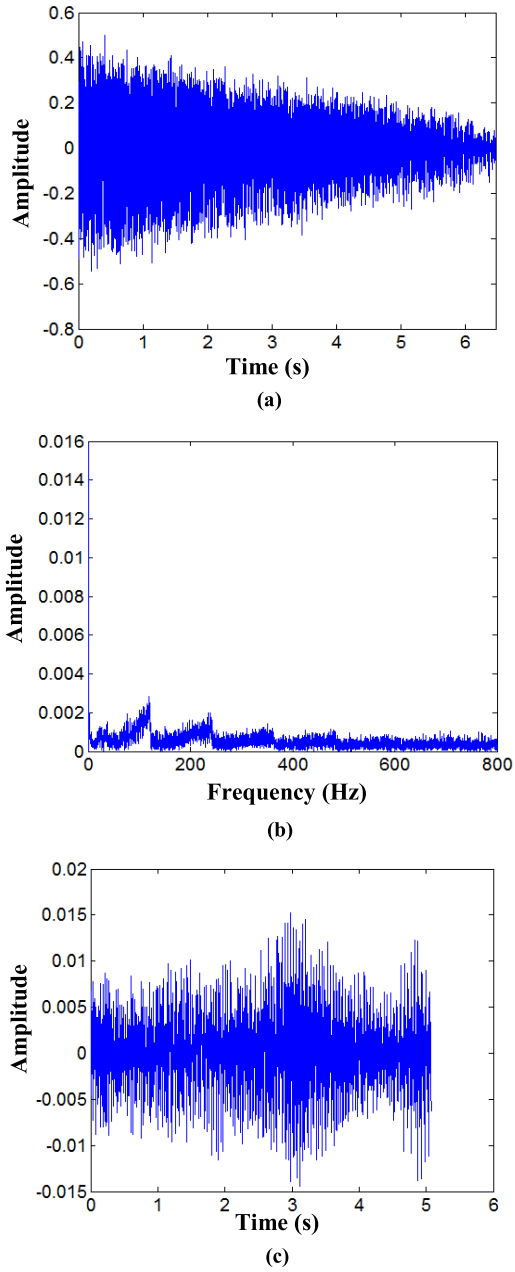

FIGURE 13. Raw signal of rolling element bearing with an outer race fault under variable speed conditions: (a) waveform of the raw signal, (b) spectrum of the raw signal, (c) waveform of the down-sampled signal.

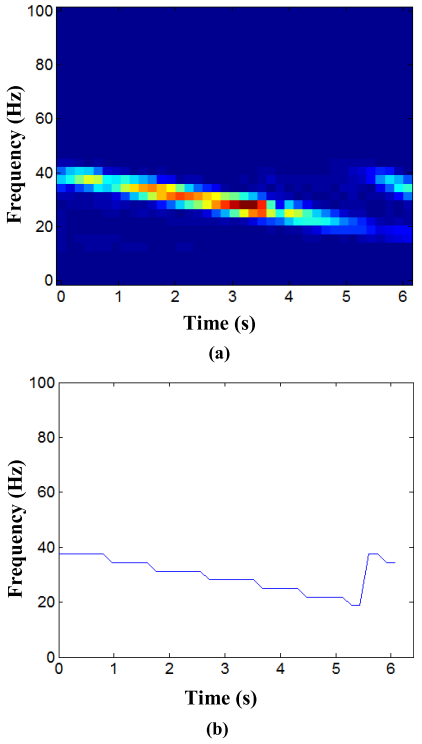

FIGURE 14. Rolling element bearing with an outer race fault: (a) spectrogram of the raw signal based STFT, (b) estimation IRF curve based the obtained TFR by STFT.

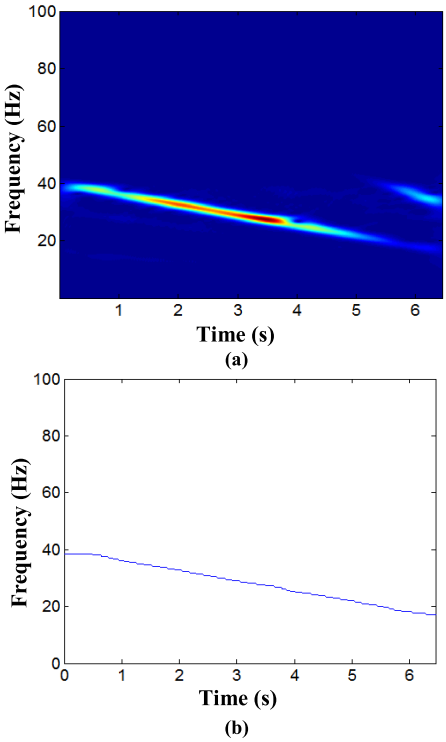

FIGURE 15. Rolling element bearing with an outer race fault: (a) spectrogram of the raw signal based GLCT, (b) estimation IRF curve based the obtained TFR by GLCT.

spectrum of the filtered signal by the AW algorithm. The order spectrum of the ASA is shown in Fig. 5(d), and only the shaft order 1.015 is detected. Fig. 5(e) is similar to Fig. 5(c), without any fault information, which is provided by WHT. Fig. 5(f) presents the order spectrum of the purified signal by ACVTD, and the order spectrum peaks of 2.3 and 6.6 are approximately $1 \times B$ and $2 \times B$, respectively. The comparison results indicate that the proposed method is better than the aforementioned methods in signal processing.

Fig. 6(a) shows the waveform of the simulated faulty signal with different white Gaussian noises (with an SNR of -6.9 dB) of Eq. (18). To test the anti-noise ability of the ACVTD method, we only show the order spectrum of the denoised signal. From Fig.6 (b), the peak values of 6.5 and 13.2 are approximately $2 \times B$ and

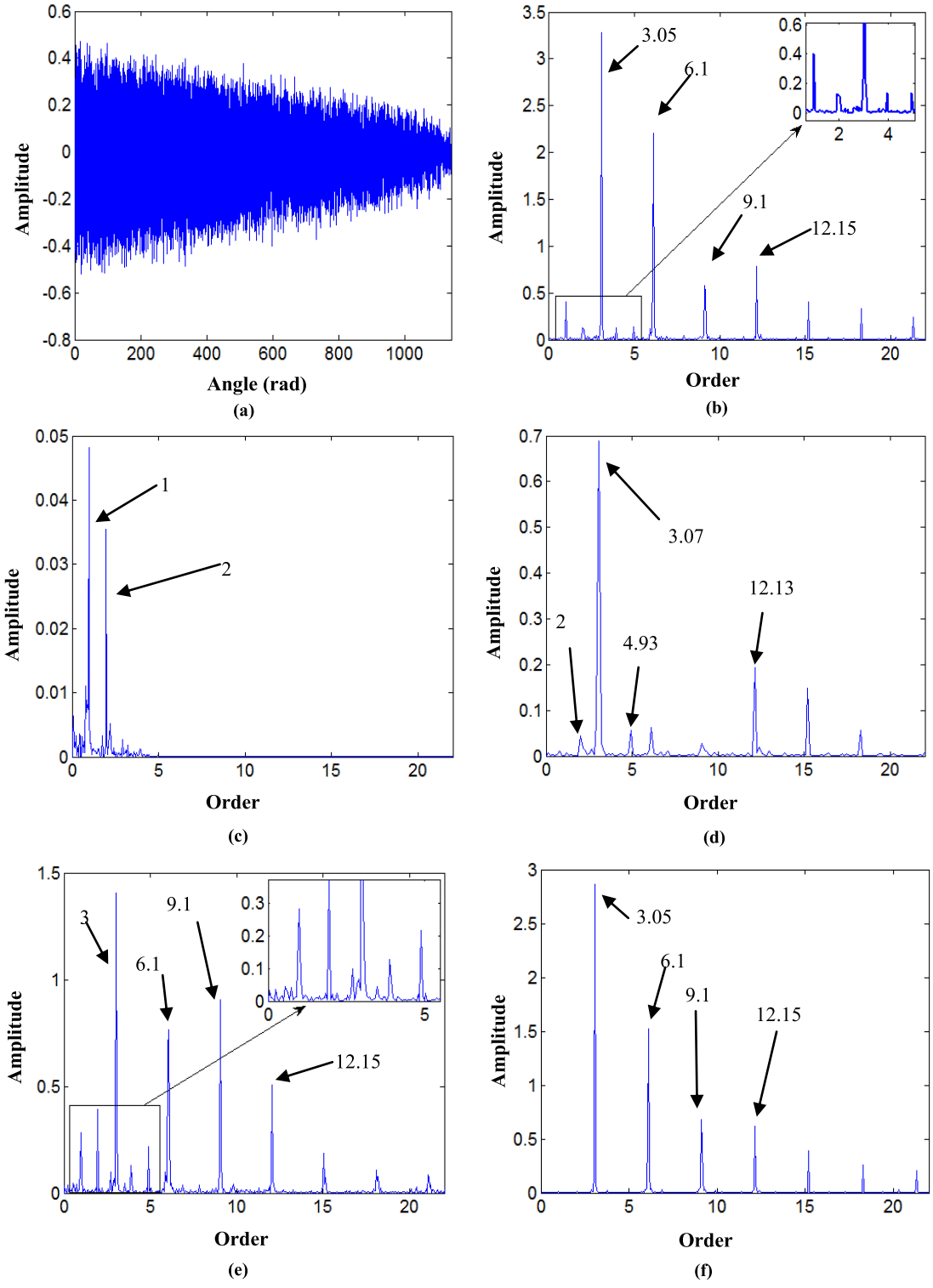

FIGURE 16. Angular domain signal: (a) waveform of the angular domain signal, (b) order spectrum of the angular domain signal, (c) order spectrum of AW output signal, (d) order spectrum of ASA output signal, (e) order spectrum of WHT output signal, (f) order spectrum of ACVTD output signal.

$3 \times B$, respectively. The anti-noise ability of the ACVTD method is verified in two different white Gaussian noise conditions.

In this work, a simulated faulty signal with SNR of 0 dB is given and its waveform of raw signal is shown in Fig. 7(a). Due to without adding any contaminants in signal,

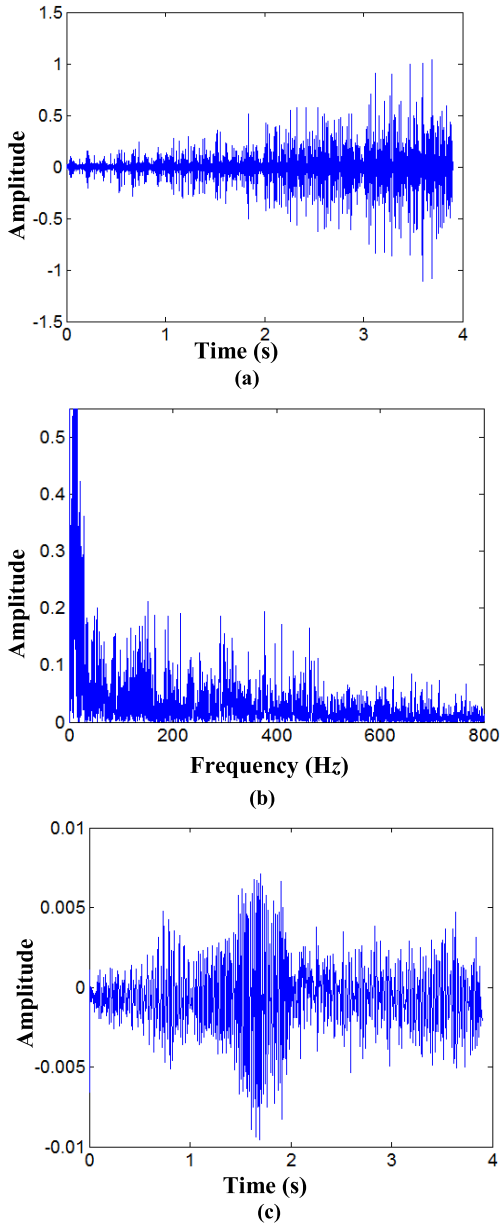

FIGURE 17. Raw signal of rolling element bearing with a defect on ball under variable speed conditions: (a) waveform of the raw signal, (b) spectrum of the raw signal, (c) waveform of the down-sampled signal.

the figure clearly presents variable interval of fault impulse. The order spectrum of the proposed method is shown in Fig. 7(b), which effectively presents the fault features 2.2 and 4.3.

V. EXPERIMENTAL VERIFICATION

In this section, the effectiveness of the proposed method is further verified with the experimental rolling element bearings under variable speed conditions, which include inner and outer race faults, ball faults and a normal case. Both experimental rolling element bearings are ER-12K.

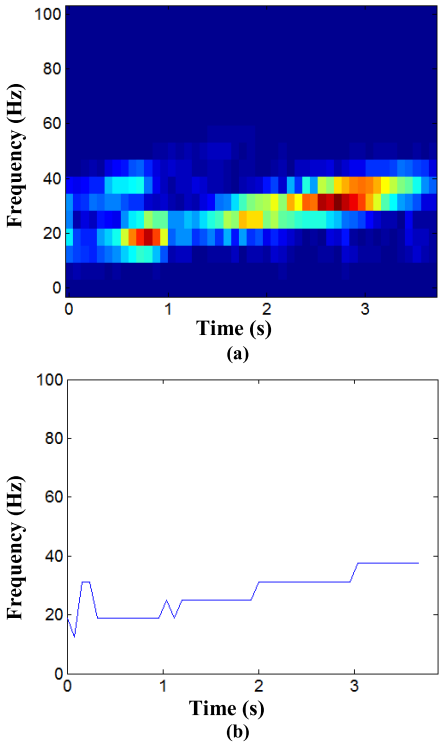

FIGURE 18. Rolling element bearing with a defect on ball: (a) spectrogram of the raw signal based STFT, (b) estimation IRF curve based the obtained TFR by STFT.

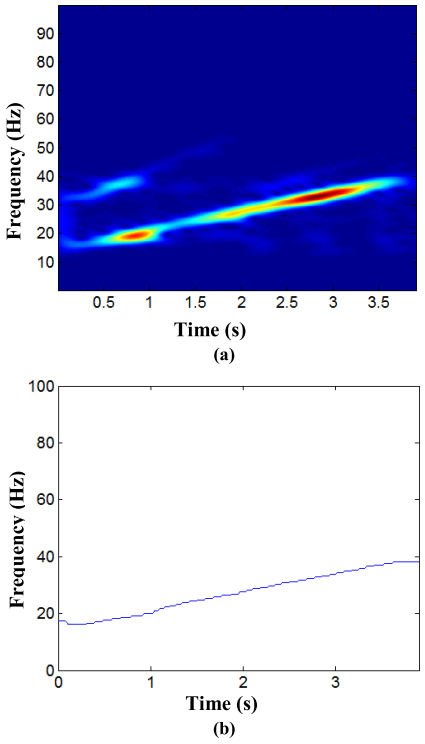

FIGURE 19. Rolling element bearing with a defect on ball: (a) spectrogram of the raw signal based GLCT, (b) estimation IRF curve based the obtained TFR by GLCT.

We set the sampling frequency 25.6 kHz. The detailed parameters of the experimental rolling element bearings are given in Table 1. The formulas of the theoretical fault

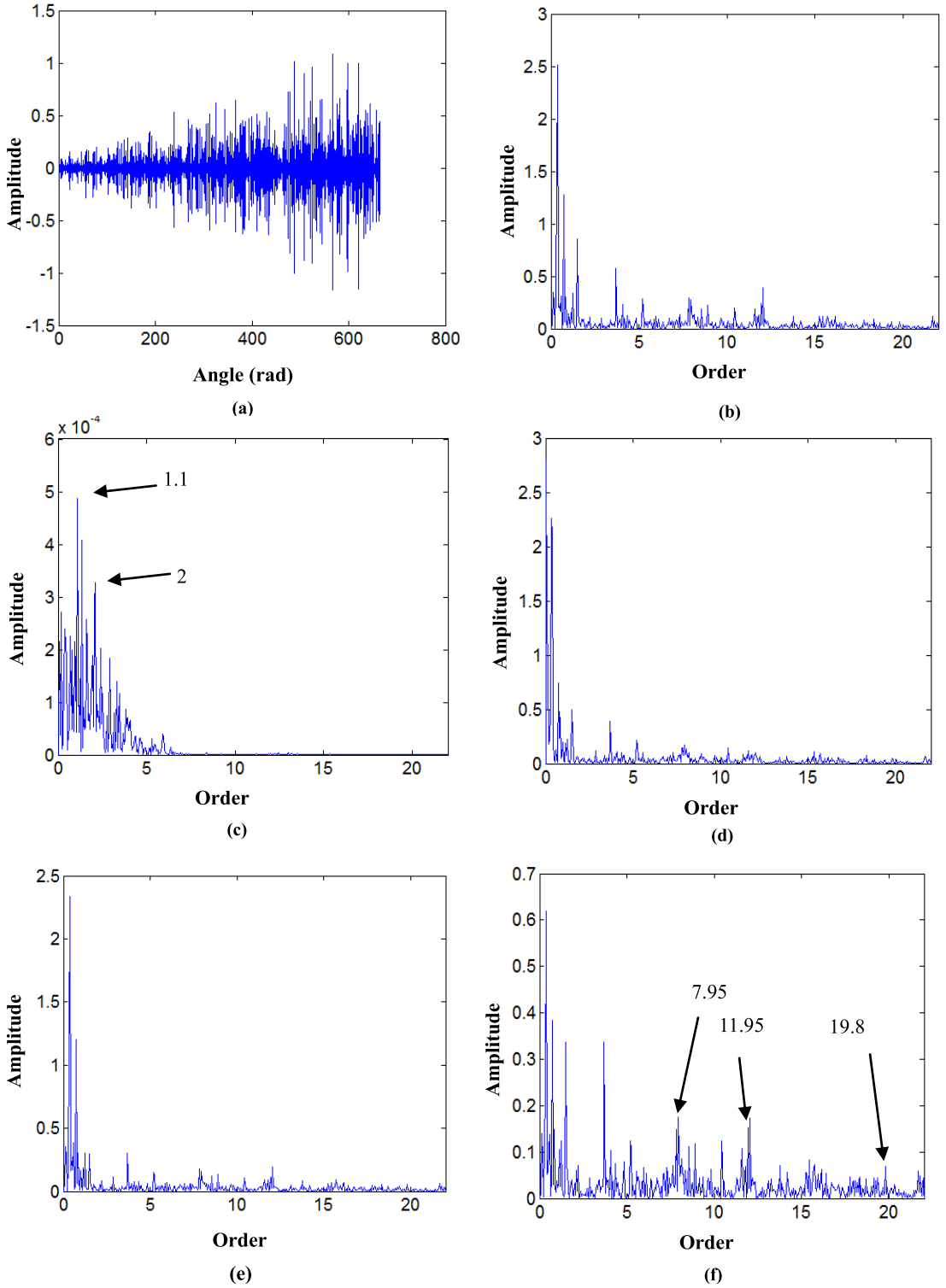

FIGURE 20. Angular domain signal: (a) waveform of the angular domain signal, (b) order spectrum of the angular domain signal, (c) order spectrum of AW output signal, (d) order spectrum of ASA output signal, (e) order spectrum of WHT output signal, (f) order spectrum of ACVTD output signal.

characteristic order of the inner race and outer race are given as

$$f_{inner} = \frac{Z}{2}(1 + \frac{d}{D}\cos\theta)f_r \tag{20}$$

$$f_{outerr} = \frac{Z}{2}(1 - \frac{d}{D}\cos\theta)f_r \tag{21}$$

$$f_{ball} = \frac{1}{2}\frac{D}{d}[1 - (\frac{d}{D})^2\cos^2\theta] \tag{22}$$

TABLE 1. Parameters of the tested rolling element bearings.

Bearing type	Ball number Z	Pitch diameter D (*mm*)	Ball diameter d (*mm*)	Contact angle θ (°)	Accelerometers 1#, 2# (mV/g)	Motor load (HP)
EK-12K	8	33.4772	7.9375	0	98	1

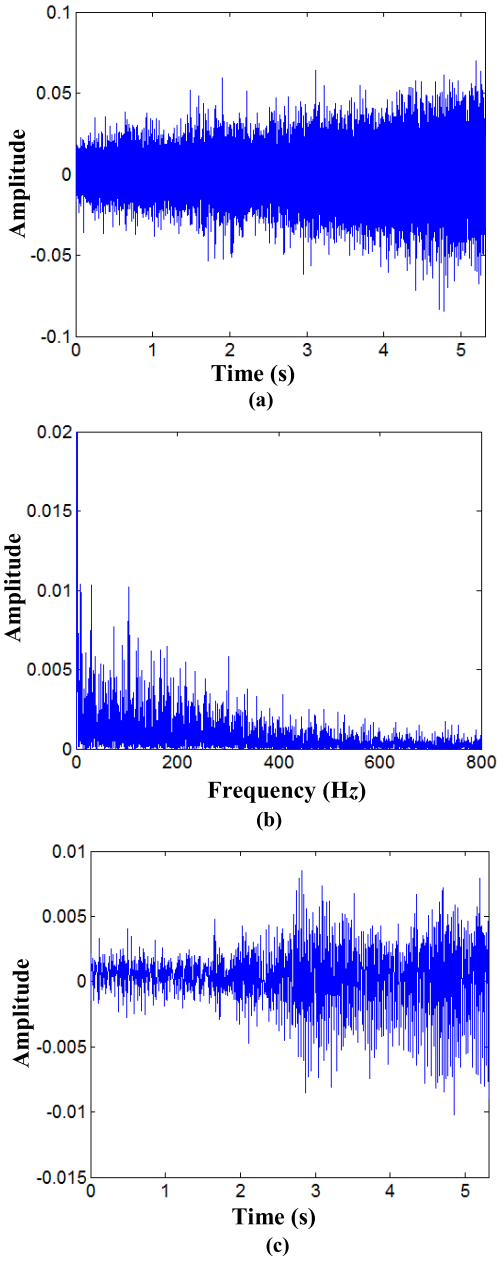

FIGURE 21. Raw signal of normal rolling element bearing under variable speed conditions: (a) waveform of the raw signal, (b) spectrum of the raw signal, (c) waveform of the down-sampled signal.

where f_r denotes the shaft frequency. Substituting the detailed parameters of the rolling element bearing into the Eq. (20)-(22), the formulas are rewritten as

$$f_{inner} = 4.95 f_r \tag{23}$$

$$f_{outer} = 3.05 f_r \tag{24}$$

$$f_{ball} = 1.99 f_r \tag{25}$$

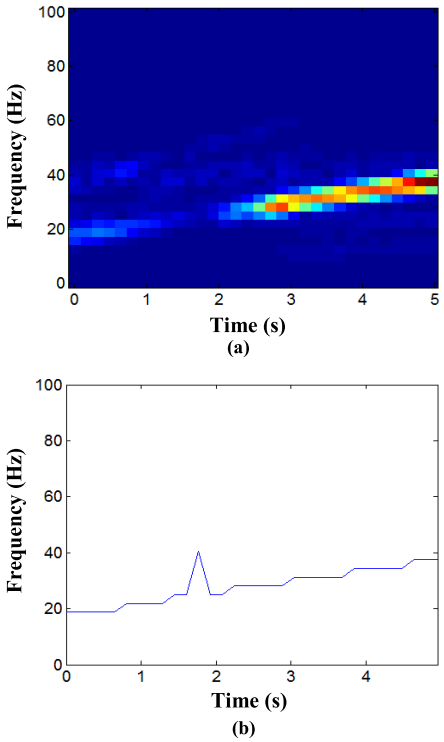

FIGURE 22. Normal rolling element bearing: (a) spectrogram of the raw signal based STFT, (b) estimation IRF curve based the obtained TFR by STFT.

As a consequence, the fault characteristic order of the inner race is 4.95, and the fault characteristic order of the outer race is 3.05, and the fault characteristic order of the ball is 1.99.

A. INNER RACE FAULT DETECTION

In this section, a rolling element bearing with a localized fault is tested. The length of the collected signal is12.8 *s* and the range of speed variation is set to 0-2400 rev/min. We select 153600 samples as the tested signal. Thus, the central frequency and bandwidth parameters of the band-pass filter can be set as 28 Hz and 28 Hz, respectively. The waveform of the tested signal is shown in Fig. 9(a) and its envelope spectrum is shown in Fig. 9(b). The fault information cannot be extracted directly due to the speed variation and heavy background noises.

For fault extraction under non-stationary conditions, the tested signal is down-sampled and the sampling frequency is decimated at $1/128$ times 25600 Hz. The waveform of the down-sampled signal is shown in Fig. 9(c). After being filtered by the band-pass filter, the IRF curve is estimated by the time-frequency methods. STFT is applied to obtain the TFR of the filtered signal and its estimated low quality IRF curve is shown in Fig. 10(a) and (b). Fig. 11(a) displays the high quality time-frequency resolution in the time-frequency

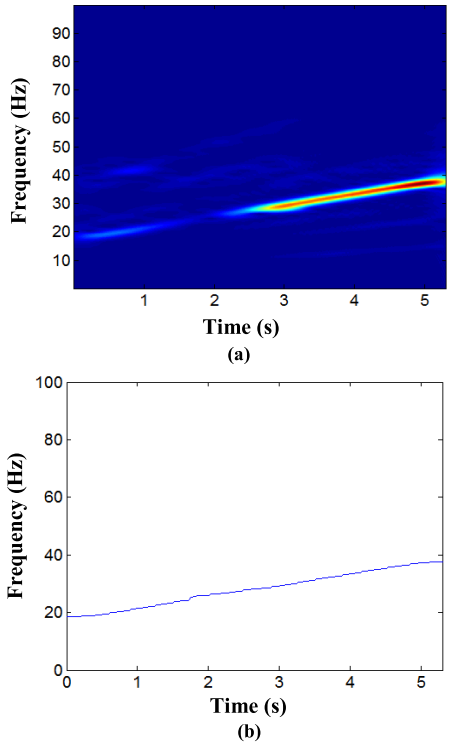

FIGURE 23. Normal rolling element bearing: (a) spectrogram of the raw signal based GLCT, (b) estimation IRF curve based the obtained TFR by GLCT.

plane using GLCT, and Fig. 11(b) shows the corresponding estimated IRF curve.

With the help of the IRF curve, the tested signal is re-sampled to the angular domain signal. Furthermore, it is similar to the numerical simulation, and sample point per rotation is 1150.5. The angular domain signal is shown in Fig. 12(a). Fig. 12(b) displays the order spectrum of the angular domain signal, for which only shaft orders 1 and 2 are detected. Fig. 12(c) shows the order spectrum of the filtered signal by the AW algorithm. Similarly, shaft orders 1 and 2 are extracted without any fault information. ASA is applied to eliminate the unrelated components and the order spectrum of the output signal by ASA is shown in Fig. 12(d). No fault features are expressed in the configuration. In Fig. 12(e), only shaft order 1 and harmonics 2 are presented, which is provided by WHT. Fig. 12(f) shows the order spectrum of the purified signal by the proposed method. Considering the theoretical FCO of the inner race, we obtain 4.95, 9.85 and 14.8 in Fig. 12(f), which correspond to $1 \times FCO$, $2 \times FCO$ and $3 \times FCO$, respectively. Meanwhile, shaft orders 1 and 2 are detected. From the comparison results, the ability of the proposed method to purify signals is testified.

B. OUTER RACE FAULT DETECTION

Similarly, the length of the collected signal is 12.8 s which is also measured in speed variation, and we choose 165600 samples as the tested signal. The rotation frequency is decreased from 40 Hz to 15 Hz. Therefore, the central frequency and bandwidth are 25 Hz and 25 Hz, respectively. Fig. 13(a) and (b) show the waveform of the tested signal and its corresponding envelope spectrum, respectively. From the configurations, no useful information can be detected. The waveform of the down-sampled signal is shown in Fig. 13(c).

The tested signal is down-sampled and the sampling frequency is reduced to 200 Hz. The TFR of the filtered signal by STFT is shown in Fig. 14(a). Fig. 14(b) shows the corresponding IRF curve estimation. Unfortunately, the estimated IRF curve is inaccurate due to the energy leakage in the low frequency plane. GLCT validly characterizes the time-varying procedure of the rotating shaft, which is displayed in Fig. 15(a). Fig. 15(b) is the corresponding IRF curve. On the basis of the IRF curve, the re-sample technique is introduced to transfer the time domain signal into the angular domain signal and the decided sample point per rotation is 1503.9.

Fig. 16(a) presents the angular domain signal, and Fig. 16(b) shows the order spectrum of the angular domain signal. On the basis of the theoretical FCO of an outer race fault, Fig. 17(b) displays the interferential orders and fault features of 3.05, 6.1, 9.1, and 12.15. The detected fault features are accompanied by the shaft order interferences. The order spectrum results of the AW algorithm and ASA are shown in Fig. 16(c) and (d), respectively, in which the former only provides shaft orders 1, 2, and the latter shows shaft and fault orders 2, 4.93 and 3.07, 12.13. From Fig. 16(e), the WHT method cannot eliminate interferential orders. In contrast, Fig. 16 (f) only exhibits 3.05, 6.1, 9.1 and 12.15, which approaches $1 \times FCO$, $2 \times FCO$, $3 \times FCO$ and $4 \times FCO$, respectively. The fault features are clearly detected without any interference. The experimental results reveal that the proposed method is available for fault detection.

C. BALL FAULT DETECTION

In this section, the proposed method is tested for the ball defection. The collected signal length is the same as that in the above two cases, and for computation efficiency, we only truncate the length to 3.9 s for the tested signal. The speed range is set between 600-2400 *rev/min*, and thus, the central frequency and bandwidth parameters of the band-pass filter are set as 24 Hz and 20 Hz, respectively. Fig. 17(a) and (b) show the waveform of the raw signal and the corresponding envelope spectrum. No fault information can be detected in the above two configurations. To eliminate influence of the speed variation of the shaft, we will transform the raw signal into the angular domain. The first step is to down-sample the raw signal then the sampling frequency is decreased to 200 Hz. The waveform of the down-sampled signal is shown in Fig. 17(c).

STFT is applied to calculate the TFR of the filtered signal, and its result is shown in Fig. 18(a). Fig. 18(b) shows the corresponding estimated IRF curve. Apparently, the curve is inaccurate, which is the result of the poor time-frequency resolution of STFT. Fig. 19(a) displays the rotation frequency component of the filtered signal in the time-frequency plane using the GLCT method. The corresponding IRF curve

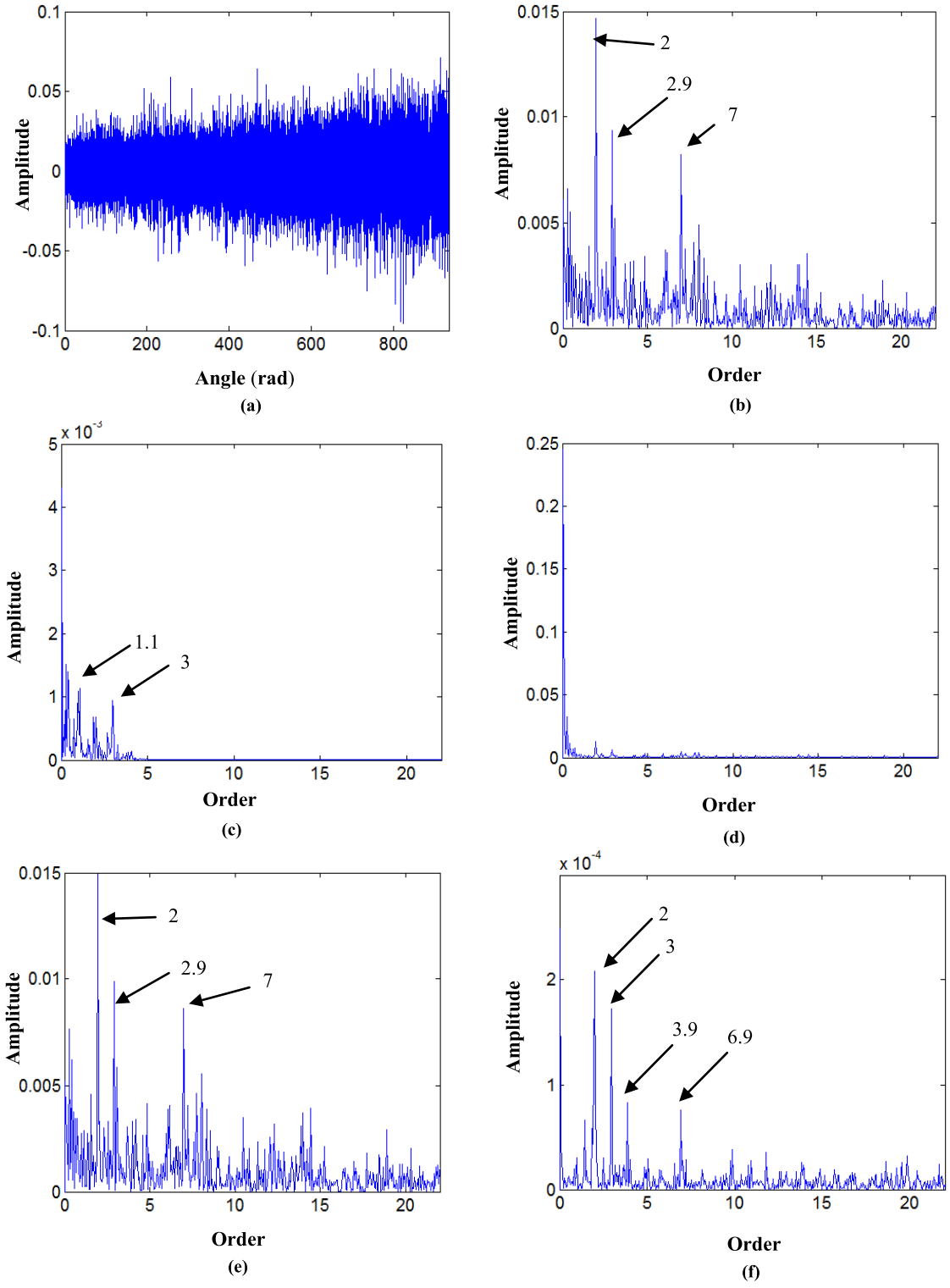

FIGURE 24. Angular domain signal: (a) waveform of the angular domain signal, (b) order spectrum of the angular domain signal, (c) order spectrum of AW output signal, (d) order spectrum of ASA output signal, (e) order spectrum of WHT output signal, (f) order spectrum of ACVTD output signal.

estimation is presented in Fig. 19(b). Obviously, the GLCT method effectively characterizes the shaft speed variation.

With the help of the extracted IF curve, we obtain the sample point per rotation is 1562.7 according to the minimum IRF. The raw signal is transferred into the angular domain by even-angle increments. The angular domain signal is shown in Fig. 20(a), and its envelope spectrum is presented in Fig. 20(b). Although there are several peaks in the order

spectrum, none of them belong to fault features. Only the shaft order and its harmonic are shown in Fig. 20 (c) using the AW method. The order spectrum results of the ASA and WHT methods are shown in Fig. 20(d) and (e), which are similar to Fig. 20(b). The ACVTD method has the ability to separate the fault components from synthetic signals. The effectiveness of ACVTD is testified by filtering the angular domain signal; the corresponding order spectrum result is shown in Fig. 20(f). Referencing the theoretical FCO of a ball fault of 1.99, the extracted three peaks of 7.95, 11.95 and 19.8 approach $4 \times FCO$, $6 \times FCO$ and $10 \times FCO$, respectively. From the above comparison results, it is easily verified that ACVTD is an available method to highlight fault components

D. NORMAL CASE

Unlike the above three experiments, the healthy bearing is installed, and its operation conditions are also variable. In this experiment, the range of the shaft speed is 900-2400 rev*/min,* and the signal lasts for 5.27 *s*. The present technique is again applied to process the collected raw signal. Fig. 21(a) and (b) display the waveform of the raw signal and its corresponding envelope spectrum. No useful information can be detected from the two configurations. The waveform of the down-sampled signal is shown in Fig. 21(c).

In the same way, the vibration signal is down-sampled and the sampling frequency is reduced to 200 H*z*. We set the central frequency and bandwidth to 28 H*z*, which are decided by the range of the shaft speeds in the data acquisition process. STFT provides a poor time-frequency in Fig. 22(a), which leads to the inaccurate result in Fig. 22(b). In contrast, Fig. 23(a) clearly exhibits the time-varying procedure of the rotating shaft, which is obtained by the GLCT method. The corresponding estimated if curve is shown in Fig. 23(b).

On the basis of the extracted IRF curve, we re-sample the raw signal into the angular domain by the re-sampling technique with even-angle increments (the sample point per rotation is 1396.7). Fig. 24(a) and (b) display the angular domain signal and its order spectrum. Except shaft orders 2, 2.9 and 7, which are easily detected, many unrelated components are introduced at the same time. Only the shaft order 1.1 and its harmonic 3 are presented in Fig. 24(c), and we would not find more related information in the order spectrum. There are no clear peak values at the shaft order harmonics in Fig. 24(d), which is processed by the ASA method. Comparing Fig. 24(e) with Fig. 24(b), the result obtained by wht is similar to that of the classical method. ACVTD is applied to eliminate the unrelated components; the corresponding order spectrum is shown in Fig. 24(f). Unlike Fig. 24(b) and (e), the shaft order harmonics 2, 3, 3.9 and 6.9 are clearly detected without any interference. Although most of the aforementioned methods can extract features, we will calculate the SNR of the filtered signal to further verify the anti-noise ability of the ACVTD method. The AW, ASA, WHT and ACVTD methods corresponding results are shown: -3 dB, -14.3 dB, 9.7 db, and -22 dB. From the obtained results, the filtered signal by WHT has the highest SNR. However, the unrelated components are introduced simultaneously to impact the ability of features extraction.

VI. DISSCUSSION

The effectiveness and superiority of the ACVTD based EOS method has been validated from the numerical simulation and experimental results. In this paper, the characteristics of the collected raw signal are non-stationary under variable speed conditions. By means of the TLOT technique based on GLCT, the raw non-stationary signal is transferred to the angular domain by the re-sampling technique. We avoid installing any hardware equipment in industrial applications to obtain rotation speed information. However, the errors of the actual and estimated speeds become bigger when the tested elements change speed rapidly.

In the quasi-stationary domain, ACVTD is applied to purify the angular domain signal to enhance the performance of the EOS method. This method has some advantages, for example, the signal can be processed automatically with high flexibility and adaptability, and it does not rely on any prior knowledge of the tested signal for fault diagnosis. Nevertheless, this method consists of two parts (for kurtosis computation and threshold searching), which may increase the calculation costs.

VII. CONCLUSION

A method has been proposed to extract the fault characteristic orders of rolling element bearings under variable speed conditions. The procedures of the present method include the following: (1) GLCT is employed to generate the time-frequency representation of the raw signals of bearings to obtain a high resolution IRF curve. (2) On basis of the extracted IRF curve, the raw signal is re-sampled into the angular domain. (3) To purify the angular domain signal, the ACVTD algorithm is applied based on its powerful adaptive noise cancellation ability without any prior knowledge of noise level. (4) The EOS method is finally employed to extract the FCO. The performance of the present method is verified by numerical simulations and experimental investigations. Compared with AW, ASA and WHT, the ability of the proposed method to accurately extract FCO is superior.

It is expected that the proposed method can be extended to the non-stationary signal processing of vibrations, acoustics, currents, temperatures, etc.

REFERENCES

[1] H. Liu and J. Xiang, "A strategy using variational mode decomposition, L-kurtosis and minimum entropy deconvolution to detect mechanical faults," *IEEE Access*, vol. 7, pp. 70564–70573, 2019.

[2] A. Kumar and R. Kumar, "Adaptive artificial intelligence for automatic identification of defect in the angular contact bearing," *Neural Comput. Appl.*, vol. 29, no. 8, pp. 277–287, Apr. 2018.

[3] G. Mirzaeva and K. I. Saad, "Advanced diagnosis of stator turn-to-turn faults and static eccentricity in induction motors based on internal flux measurement," *IEEE Trans. Ind. Appl.*, vol. 54, no. 4, pp. 3961–3970, Jul./Aug. 2018.

[4] J. Yoon, D. He, and B. Van Hecke, "On the use of a single piezoelectric strain sensor for wind turbine planetary gearbox fault diagnosis," *IEEE Trans. Ind. Electron.*, vol. 62, no. 10, pp. 6585–6593, Oct. 2015.
[5] L. Song, H. Wang, and P. Chen, "Vibration-based intelligent fault diagnosis for roller bearings in low-speed rotating machinery," *IEEE Trans. Instrum. Meas.*, vol. 67, no. 8, pp. 1887–1899, Aug. 2018.
[6] P. J. Kootsookos, B. C. Lovell, and B. Boashash, "A unified approach to the STFT, TFDs, and instantaneous frequency," *IEEE Trans. Signal Process.*, vol. 40, no. 8, pp. 1971–1982, Aug. 1992.
[7] H. Ahmed and A. K. Nandi, "Compressive sampling and feature ranking framework for bearing fault classification with vibration signals," *IEEE Access*, vol. 6, pp. 44731–44746, 2018.
[8] S. K. Lee and P. R. White, "Higher-order time-frequency analysis and its application to fault detection in rotating machinery," *Mech. Syst. Signal Process.*, vol. 11, no. 4, pp. 637–650, Jul. 1997.
[9] K. R. Fyfe and E. D. S. Munck, "Analysis of computed order tracking," *Mech. Syst. Signal Process.*, vol. 11, no. 2, pp. 187–205, Mar. 1997.
[10] M. Zhao, J. Lin, X. Wang, Y. Lei, and J. Cao, "A tacho-less order tracking technique for large speed variations," *Mech. Syst. Signal Process.*, vol. 40, no. 1, pp. 76–90, Oct. 2013.
[11] Y. Wang, B. Tang, L. Meng, and B. Hou, "Adaptive estimation of instantaneous angular speed for wind turbine planetary gearbox fault detection," *IEEE Access*, vol. 7, pp. 49974–49984, 2019.
[12] Z. Feng, F. Chu, and M. J. Zuo, "Time-frequency analysis of time-varying modulated signals based on improved energy separation by iterative generalized demodulation," *J. Sound Vib.*, vol. 330, no. 6, pp. 1225–1243, Mar. 2011.
[13] Q. Leclère, H. André, and J. Antoni, "A multi-order probabilistic approach for instantaneous angular speed tracking debriefing of the CMMNO'14 diagnosis contest," *Mech. Syst. Signal Process.*, vol. 81, pp. 375–386, Dec. 2016.
[14] M. Zhao, J. Lin, X. Xu, and Y. Lei, "Tacholess envelope order analysis and its application to fault detection of rolling element bearings with varying speeds," *Sensors*, vol. 13, no. 8, pp. 10856–10875, 2013.
[15] M. Garrido, "The feedforward short-time Fourier transform," *IEEE Trans. Circuits Syst. II, Exp. Briefs*, vol. 63, no. 9, pp. 868–872, Sep. 2016.
[16] A. Nuruzzaman, O. Boyraz, and B. Jalali, "Time-stretched short-time Fourier transform," *IEEE Trans. Instrum. Meas.*, vol. 55, no. 2, pp. 598–602, Apr. 2006.
[17] A. Bouzida, O. Touhami, R. Ibtiouen, A. Belouchrani, M. Fadel, and A. Rezzoug, "Fault diagnosis in industrial induction machines through discrete wavelet transform," *IEEE Trans. Ind. Electron.*, vol. 58, no. 9, pp. 4385–4395, Sep. 2011.
[18] C. Min, G. Wen, B. Li, and F. Fan, "Blind deblurring via a novel recursive deep CNN improved by wavelet transform," *IEEE Access*, vol. 6, pp. 69242–69252, 2018.
[19] S. Qian and D. Chen, "Decomposition of the Wigner-Ville distribution and time-frequency distribution series," *IEEE Trans. Signal Process.*, vol. 42, no. 10, pp. 2836–2842, Oct. 1994.
[20] K. Cai, W. Cao, L. Aarniovuori, H. Pang, Y. Lin, and G. Li, "Classification of power quality disturbances using Wigner-Ville distribution and deep convolutional neural networks," *IEEE Access*, vol. 7, pp. 119099–119109, 2019.
[21] Z. Feng, X. Chen, and T. Wang, "Time-varying demodulation analysis for rolling bearing fault diagnosis under variable speed conditions," *J. Sound Vib.*, vol. 400, pp. 71–85, Jul. 2017.
[22] G. Yu and Y. Zhou, "General linear chirplet transform," *Mech. Syst. Signal Process.*, vols. 70–71, pp. 958–973, Mar. 2016.
[23] Y. Wang, L. Yang, J. Xiang, J. Yang, and S. He, "A hybrid approach to fault diagnosis of roller bearings under variable speed conditions," *Meas. Sci. Technol.*, vol. 28, no. 12, Dec. 2017, Art. no. 125104.
[24] L. Wang, J. Xiang, and Y. Liu, "A time-frequency-based maximum correlated kurtosis deconvolution approach for detecting bearing faults under variable speed conditions," *Meas. Sci. Technol.*, vol. 30, no. 12, Dec. 2019, Art. no. 125005.
[25] L. Wang and J. Xiang, "A two-stage method using spline-kernelled chirplet transform and angle synchronous averaging to detect faults at variable speed," *IEEE Access*, vol. 7, pp. 22471–22485, 2019.
[26] X. Wang, F. Zhou, Y. He, and Y. Wu, "Weak fault diagnosis of rolling bearing under variable speed condition using IEWT-based enhanced envelope order spectrum," *Meas. Sci. Technol.*, vol. 30, no. 3, Mar. 2019, Art. no. 035003.
[27] S. M. Mousavi and C. A. Langston, "Automatic noise-removal/signal-removal based on general cross-validation thresholding in synchrosqueezed domain and its application on earthquake data," *Geophysics*, vol. 82, no. 4, pp. V211–V227, Jul. 2017.
[28] W. Zhu, S. M. Mousavi, and G. C. Beroza, "Seismic signal denoising and decomposition using deep neural networks," *IEEE Trans. Geosci. Remote Sens.*, vol. 57, no. 11, pp. 9476–9488, Nov. 2019.
[29] A. Djebala, M. K. Babouri, and N. Ouelaa, "Rolling bearing fault detection using a hybrid method based on empirical mode decomposition and optimized wavelet multi-resolution analysis," *Int. J. Adv. Manuf. Technol.*, vol. 79, nos. 9–12, pp. 2093–2105, Aug. 2015.
[30] A. Djebala, N. Ouelaa, C. Benchaabane, and D. F. Laefer, "Application of the wavelet multi-resolution analysis and Hilbert transform for the prediction of gear tooth defects," *Meccanica*, vol. 47, no. 7, pp. 1601–1612, Oct. 2012.
[31] G. Thakur and H.-T. Wu, "Synchrosqueezing-based recovery of instantaneous frequency from nonuniform samples," *SIAM J. Math. Anal.*, vol. 43, no. 5, pp. 2078–2095, Jan. 2011.
[32] I. Daubechies, J. Lu, and H.-T. Wu, "Synchrosqueezed wavelet transforms: An empirical mode decomposition-like tool," *Appl. Comput. Harmon. Anal.*, vol. 30, no. 2, pp. 243–261, Mar. 2011.
[33] S. K. Ghosh, R. K. Tripathy, R. N. Ponnalagu, and R. B. Pachori, "Automated detection of heart valve disorders from the PCG signal using time-frequency magnitude and phase features," *IEEE Sensors Lett.*, vol. 3, no. 12, pp. 1–4, Dec. 2019.
[34] S. Madhavan, R. K. Tripathy, and R. B. Pachori, "Time-frequency domain deep convolutional neural network for the classification of focal and non-focal EEG signals," *IEEE Sensors J.*, vol. 20, no. 6, pp. 3078–3086, Mar. 2020.
[35] T. Al-Attar and S. V. Madihally, "Modeling the impact of fluid flow on resveratrol release from electrospun fibers," *Comput. Biol. Med.*, vol. 117, Feb. 2020, Art. no. 103622.

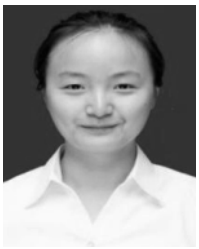

YI LIU received the B.S. degree in automobile support engineering from the Heilongjiang Institute of Technology, China, in 2017. She is currently pursuing the master's degree in mechanical engineering with the Guilin University of Electronic Technology and jointing training in Wenzhou University. Her research interests include fault detection of mechanical systems, and vibration analysis.

ZHANSI JIANG received the B.S. degree in mechanical engineering from the Inner Mongolia University of Science and Technology, China, in 2001, the M.S. degree from Guangxi University, China, in 2004, and the Ph.D. degree from the Huazhong University of Science and Technology, China, in 2008. He is currently a Professor with the School of Mechanical and Electrical Engineering, Guilin University of Electronic Technology, China. His research interests include optimization algorithm and structural health monitoring.

JIAWEI XIANG (Member, IEEE) received the B.S. degree in mechatronics from Hunan University, China, in 1997, the M.S. degree from Guangxi University, China, in 2003, and the Ph.D. degree from Xi'an Jiaotong University, China, in 2006. He is currently a Professor with the College of Mechanical and Electrical Engineering, Wenzhou University, China. His research interests include condition monitoring of mechanical systems, structural health monitoring, numerical simulation, signal processing, and vibration analysis.